Kinetics of the Homogeneous Catalytic Hydrogenation of Olefins in Supercritical Carbon Dioxide Using a Fluoroacrylate Copolymer Grafted Rhodium Catalyst

Roberto Flores,[†] Zulema K. Lopez-Castillo,[†] Ibrahim Kani,[‡] John P. Fackler, Jr.,[‡] and Aydin Akgerman*[,†]

Chemical Engineering Department, Texas A&M University, College Station, Texas 77843-3122, and Chemistry Department, Texas A&M University, College Station, Texas 77843-3012

The kinetic studies on the hydrogenation of 1-octene and cyclohexene using a fluoroacrylate copolymer grafted rhodium catalyst in supercritical carbon dioxide ($scCO_2$) are reported. The reactions were investigated at temperatures between 50 and 120 °C, and pressures ranging from 172 to 241 bar. The catalyst also deactivated at these reaction conditions. For the case of 1-octene, isomerization to (*E*)2-octene and (*Z*)2-octene also occurred as side reactions. To represent the experimental data, a kinetic model was developed on the basis of reported studies about hydrogenation and isomerization of olefins in conventional solvents. It was proposed that two hydride catalytic species are formed during the kinetic cycle. Monohydride species promoted the isomerization, and dihydride species catalyzed the hydrogenation. Deactivation of the catalyst was attributed to the formation of an unsaturated olefin complex. Statistical methods were applied to discriminate among rival models. It was found that the rate-determining steps for hydrogenation and isomerization were the formation of the alkylrhodium hydride complex and the coordination of the olefin in the monohydride catalytic species, respectively.

Introduction

Many traditional organic solvents employed in homogeneous catalysis, such as benzene, toluene, methylene chloride, THF, and DMF, are being phased out as a result of U.S. FDA and U.S. EPA regulations to limit emissions of and exposures to potentially toxic and environmentally damaging compounds. Moreover, in homogeneous catalytic processes, other disadvantages include the expensive catalyst recovery and purification processes after the reaction, and the low solubility of gases in liquid solvents.[1−2]

Supercritical fluids (SCFs) have shown significant potential as an alternative to replace the common organic solvents as reaction media because of their unique physicochemical properties. Several reviews have been published explaining the fundamentals and the main advances in this new field of chemical reaction engineering.[3−8] Specifically, supercritical carbon dioxide ($scCO_2$) is an excellent alternative to conventional solvents because it is easily separated from the other components in the process stream, nonflammable, safe to human exposure, acceptable for environmental release, and capable of performing the duties of a nonpolar solvent while allowing manipulation of its solvent strength through a wide range of polarities. At supercritical conditions, its density is sufficient to provide dissolution strength, the diffusivity of solutes is higher than in liquids, and the viscosity is lower increasing the mass transfer; therefore, a hydrogenation reaction that is diffusion-limited in the solvent phase can be enhanced by carrying it out in an SCF due to higher diffusivity and elimination of gas/liquid and fluid/fluid interphases. The main drawback of using $scCO_2$ as reaction media is the scarce solubility of conventional organometallic catalysts. Therefore, efforts have been focused on the design of new catalytic materials that are miscible in $scCO_2$ under mild conditions. Particularly, fluoropolymers and silicones have moderate solubility in $scCO_2$.[9] On the basis of that, new catalysts have been developed by grafting the catalytically important ligands to a "CO_2-philic" backbone.[10−14] Catalytically active sites become available in $scCO_2$ by the fixation of "CO_2-philic" solubilizers in the periphery of the ligand.

In the present work, a novel Rh catalyst, soluble in $scCO_2$, was synthesized by attaching rhodium ligands to a fluoroacrylate copolymer. Kinetic studies on the hydrogenation of 1-octene and cyclohexene with this novel catalyst were made. It was found that the catalyst deactivated at reaction conditions. Also, 1-octene was isomerized to (*E*)2-octene and (*Z*)2-octene as side reactions, and no appreciable hydrogenation of the 2-octene isomers was detected. Finally, the kinetic model for the hydrogenation and isomerization processes was established.

Experimental Section

Materials. Organic substances were purchased from Sigma-Aldrich and used as received. Carbon dioxide and hydrogen were bought from Brazos Welding Supply and used as received. Catalyst was prepared in the Department of Chemistry at Texas A&M University and used as received.

Catalyst. The catalyst employed in the experiments was a Wilkinson-type catalyst, where a rhodium organometallic complex was grafted to a polymer soluble in $scCO_2$. Details about the synthesis of the catalyst have been given elsewhere.[15] First, the polymer was synthesized by the polymerization of 1*H*,1*H*,2*H*,2*H*-heptade-

* To whom the correspondence should be addressed. Tel: 979-845-3375. Fax: 979-845-6446. E-mail: a-akgerman@tamu.edu.

[†] Chemical Engineering Department.

[‡] Chemistry Department.

10.1021/ie0303202 CCC: $25.00
Published on Web 11/15/2003

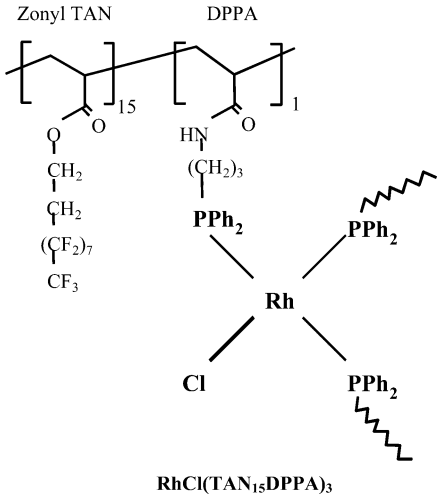

Figure 1. Ideal molecular structure of the catalyst.

cafluorodecyl acrylate monomer (zonyl TAN) and *N*-acrylosuccinimide (NASI), the former increasing the solubility in $scCO_2$ and the latter providing attachment sites for the catalyst. ^1H NMR analysis confirmed the zonyl TAN to NASI molar ratio, which was adjusted between 7 and 20. Then, the succinimide group was exchange by phosphines using $NH_2(CH_2)_3PPh_2$ (DPPA). During this step, 15−30% of the phosphines were oxidized due to uncontrolled reaction as was estimated by ^{31}P NMR analysis. Finally, this precursor was reacted with $[RhCl(COD)]_2$ to obtain the catalyst. Neutron activation analysis gave a catalyst composition of 4.4315×10^{-8} mol of Rh per gram of catalyst. The ideal molecular structure of the catalyst is presented in Figure 1.

Apparatus and Procedures. The experimental setup and procedures of operation have been described elsewhere.[16] In short, the system consisted of a 100 mL EZE-seal vessel with a magnetic drive stirrer by Autoclave Engineers and warmed with a heating jacket. The temperature was regulated using a temperature controller (Omega CN9000A) and monitored with a thermocouple (Omega 115KC) located in a thermowell inside the reactor. The pressure was measured using an Autoclave gauge. As a safety measure, a rupture disk rated at 5000 psi was installed in the reactor. Liquid CO_2 was pumped through an ice bath to the reactor using an LDC Analytical mini pump. A schematic representation of the experimental setup is given in Figure 2.

After each experimental run, the reactor was washed with acetone to remove any hydrocarbon residue, 1,1,2-trichlorotrifluoroethane to dissolve the remained catalyst, and nitric acid to eliminate any metallic catalytic deposit that could be formed during the experimentation. Finally, a mechanical cleaning was performed in all the metallic parts.

Then, a blank reaction test was performed to verify total removal of the catalyst. If conversion was obtained during the blank test, the cleaning procedure was repeated until no conversion was observed.

Samples taken from the reactor were analyzed by gas chromatography (HP 5890 equipped with a flame ionization detector) using a capillary ZB-5 column (5% Phenyl Polysiloxane, 30 m × 0.53 mm ID × 1.50 μm FT) by Phenomenex.

Hydrogenation Reaction Model. The hydrogenations of 1-octene and cyclohexene were selected to determine the activity of the catalyst. These reactions are exothermic and progress at low temperatures to reach total conversion without thermodynamic limitations. Isomerization to 2-octene and 3-octene may also occur with the Wilkinson-type catalysts. Isomerization reactions are also exothermic proceeding at mild temperatures. The initial mole fractions of all components were kept constant at all temperatures; this means that, at lower temperatures or higher pressures, where the density of $scCO_2$ is higher, the concentrations of hydrogen and olefin were greater. For the hydrogenation of 1-octene, the initial mole fractions of olefin and hydrogen were 0.0010 and 0.0334, respectively. In the case of hydrogenation of cyclohexene, the initial mole fractions of olefin and hydrogen were 0.002 and 0.056, respectively. The amount of catalyst added to the reactor was varied according to the olefin concentration. The temperature and pressure range studied were 50−95 °C and 172−241 bar. Experiments were run twice for reproducibility.

Analysis and Discussion

Estimations of the theoretical critical point of the reaction mixtures as the reactions proceeded were performed using the group contribution method for the critical temperature,[17] and the method of Liu[18] for the critical pressure. It was found that in both cases the critical temperature slightly changes from 301.47 to 301.54 K, and the critical pressure varies from 83.18 to 83.00 bar. Therefore, it can be concluded that reactions always proceed under supercritical phase conditions.

Preliminary experiments at 172 bar and different temperatures were done to determine the best substrate to catalyst molar ratio to perform parameter estimation for the hydrogenation of 1-octene. The catalyst employed was $RhCl(TAN_{15}DPPA)_3$ with 15% of oxidized phosphines. Results are presented in Figures 3 and 4. When the substrate to catalyst molar ratio was 800, excellent reaction profiles were obtained at 70 and 95 °C; however, at 50 °C almost no conversion was obtained. On the other hand, when this molar ratio decreased to 400 very fast conversion was obtained at 70 and 95 °C, but fair reaction profile was observed at 50 °C. Therefore, the selected substrate to catalyst molar ratio was 400 for experiments at 50 °C, and 800 for experiments at 70 and 95 °C.

Kinetic Mechanism. The hydrogenation of unsaturated compounds using organometallic catalyst takes place through several steps involving oxidative-addition, coordination, insertion, and reductive-elimination reactions.[19−21]

The hydrogenation mechanism goes through intermediate metal hydrides. The formation of metal hydrides typically takes place by oxidative-addition. Monometallic and bimetallic H_2 oxidative-additions are known, and both need the presence of at least one vacant site on the metal as is presented in Figure 5. Many factors influence the reactivities of metal complexes to achieve oxidative-additions. Electron-releasing ligands, i.e., phosphines, enhance the tendency to undergo oxidative-additions; in contrast, π-acceptors, such as CO or olefins, decrease the propensity to accomplish oxidative-additions. Additionally, steric inhibition is also significant, particularly with large phosphine groups. Oxidative-addition of C═C bonds is also thermodynamically possible since the energetics of C═C oxidative additions are sometimes not much different from H_2 additions. Thus,

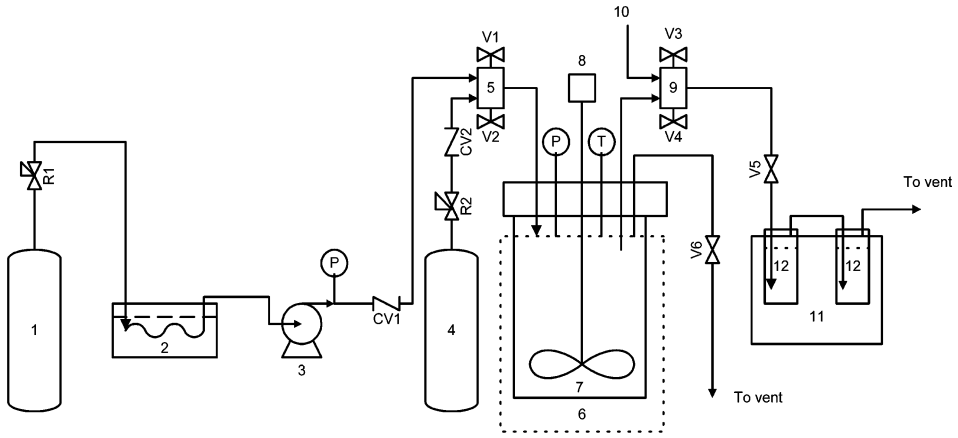

1. CO_2 Dip Tubing Cylinder
2. Ice Bath
3. MiniPump
4. H_2 Cylinder
5. Autoclave Engineers Valve
6. Autoclave Engineers Heating Jacket
7 Autoclave Engineers Reactor
8. Stirrer
9. Autoclave Engineers Valve
10. Syringe
11. Ice Bath
12. Sampling Bottles
R1-R2: Pressure Regulators
CV1-CV2: Check Valves
V1-V6: Valves

Figure 2. Schematic diagram of the reactor system.

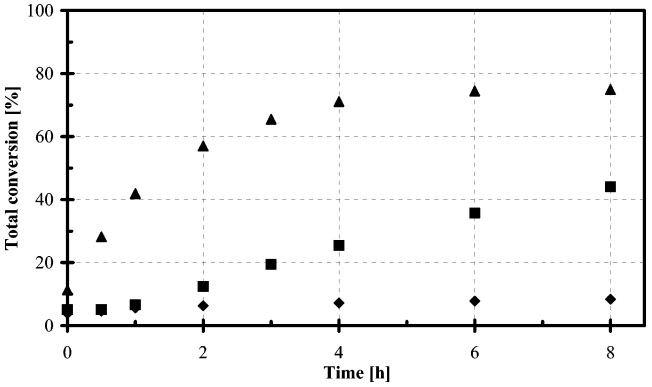

Figure 3. Preliminary experiments for the hydrogenation of 1-octene at 172 bar using a substrate to catalyst molar ratio of 800. Temperature: (◆) 50 °C, (●) 70 °C, (▲) 95 °C.

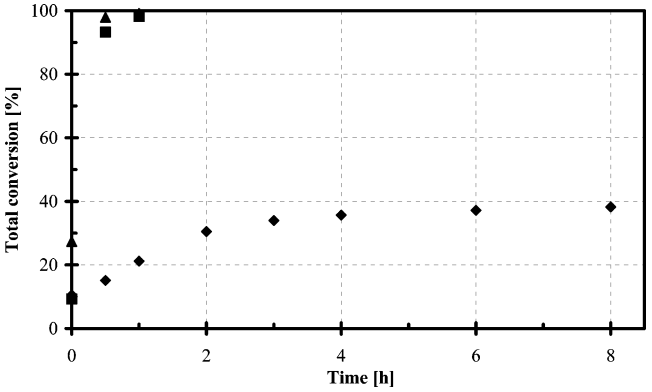

Figure 4. Preliminary experiments for the hydrogenation of 1-octene at 172 bar using a substrate to catalyst molar ratio of 400. Temperature: (◆) 50 °C, (●) 70 °C, (▲) 95 °C.

the olefin is coordinated forming an unsaturated olefin complex as is presented in Figure 6.

Once the oxidative-addition has been accomplished, these new species either coordinate an unsaturated hydrocarbon, or add H_2. However, it has been suggested that the formation of hydride olefin complexes from an unsaturated olefin complex is difficult, and in fact, the formation of an unsaturated olefin complex may tend

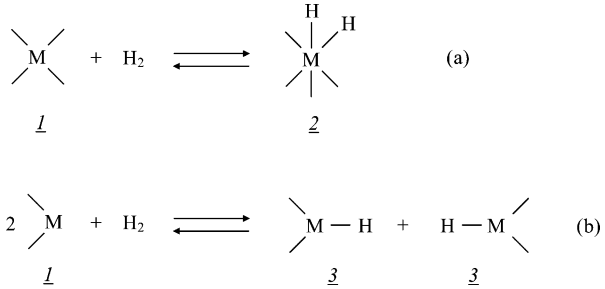

Figure 5. Oxidative-addition types of H_2 to transition metals: (a) bimetallic, (b) monometallic.

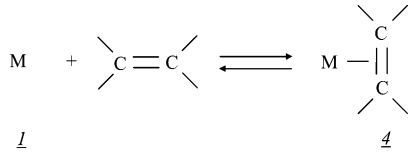

Figure 6. Formation of a catalytic inhibitor complex.

to inhibit the hydrogenation process.[22] Therefore, it is considered that only the mono- and dihydride species may continue promoting the hydrogenation and isomerization.

Homogeneous hydrogenation catalysts with dihydride complexes are much better studied and established. A generalized mechanism is given in Figure 7. Coordination of an olefin on the same face of the coordination sphere as the two hydrides provides the coordinative saturated complex **5**. The transformation of **2** to **5** requires a vacant coordination site, accounting for some of the inhibition of the catalytic cycle brought on by competing extraneous ligands. The migratory insertion of **5** to **6** goes by cis addition of the M−H bond to the olefin and requires the olefinic bond axis, the metal, and the hydride to be coplanar. This step is usually assisted or consummated by the incorporation of the external ligand. Alkyl-hydride intermediates such as **6** have rarely been observed because the following step is very rapid, preventing buildup of **6** giving high stereoselectivity and the absence of olefin rearrangement.

From the preceding explanation, it could be concluded that dihydride catalytic species would not produce

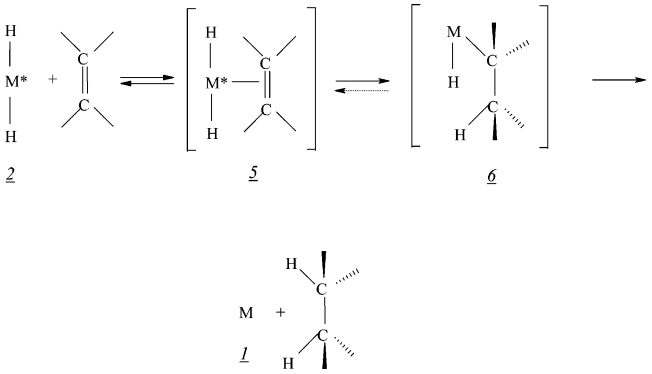

Figure 7. Mechanism of hydrogenation of olefins with dihydride catalysts.

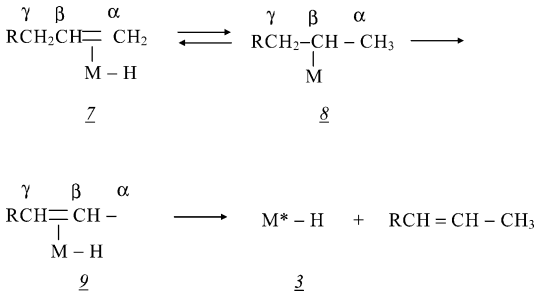

Figure 8. Mechanism of isomerization of olefins with monohydride catalysts.

isomers; therefore, a different catalytic species should be generated to produce isomers. This species could be a rhodium monohydride complex, which is an excellent isomerization catalyst.[23] The formation of this complex is uncertain, but it has been proposed that it may proceed through heterolytic dihydrogen activation to finally obtain a monohydride Rh^{I} catalytic species.[23,24] For simplification in the deduction of the kinetic mechanism, it could be assumed that the generation of this complex proceeds in a single step as it was presented in Figure 5b. Once the monohydride species has been formed, the next step involves complexation of the olefin to a coordinatively unsaturated hydride, **7**, followed by a Markovnikov hydride migration, complex **8**, as is presented in Figure 8. Then, γ-H (not α-H) elimination would take place to produce an internal olefin as is depicted in Figure 8.[2]

Table 1. Rate-Determining Steps for Hydrogenation and Isomerization in the Proposed Models

	rate-determining step	
model	hydrogenation	isomerization
1	4	9, 13
2	3	9, 13
3	2	9, 13
4	4	8, 12
5	3	8, 12
6	2	8, 12
7	4	7, 11
8	3	7, 11
9	2	7, 11
10	4	6, 10
11	3	6, 10
12	2	6, 10

Finally, it was considered that the catalyst was inhibited due to the formation of an unsaturated olefin complex as it was presented in Figure 6. The way this complex is formed is uncertain; it could be either by oxidative-addition to form a metallacyclopropane-type complex, or by simple coordination of the double bond to the metal. For simplicity, the last reaction was assumed. This complex could further react to produce dimer species that could be precipitated during the reaction.

Figure 9 presents the proposed reaction mechanism for the production of *n*-octane and 2-octene isomers. Here, the cycle for the generation of isomer must be repeated twice with different rate constants, one for the production of (*E*)2-octene, and the other for the production of (*Z*)2-octene; this is the reason that two reaction constants appear in the different reaction steps.

Parameter Estimation. For determining the kinetic model for the hydrogenation of 1-octene, models were proposed assuming different combinations of rate-determining steps for hydrogenation and isomerization reactions as is summarized in Table 1. Because hydrogen was fed with huge excess with respect to olefin, steps 1 for hydrogenation and 5 for isomerization were discarded as rate-controlling steps. Moreover, considering any of these steps as rate-controlling would lead to obtaining a kinetic expression just in terms of hydrogen concentration (without effect of the olefin concentration), and since hydrogen is in great excess, this kinetic expression would be meaningless.

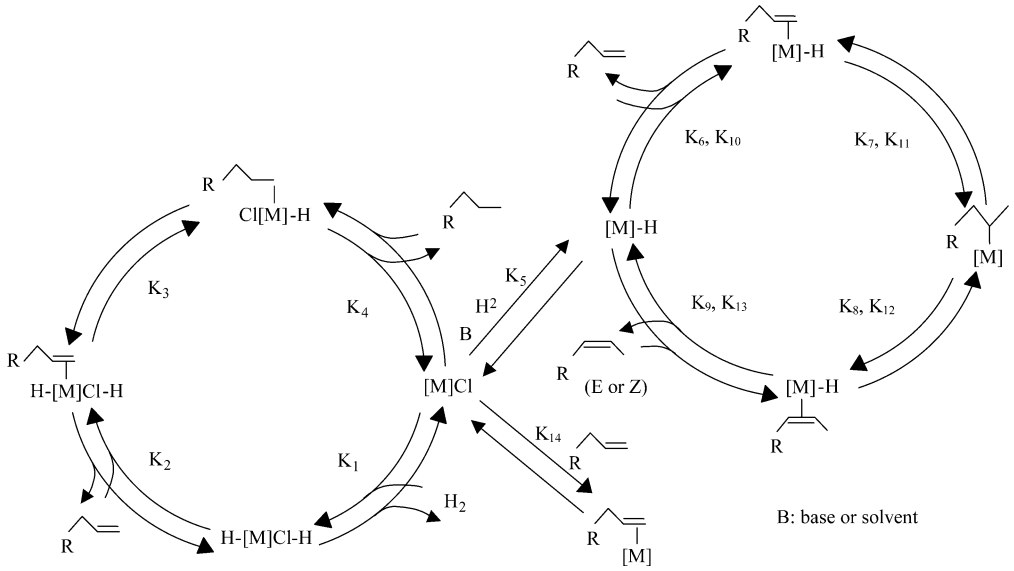

Figure 9. Reaction mechanism for the hydrogenation and isomerization of 1-octene.

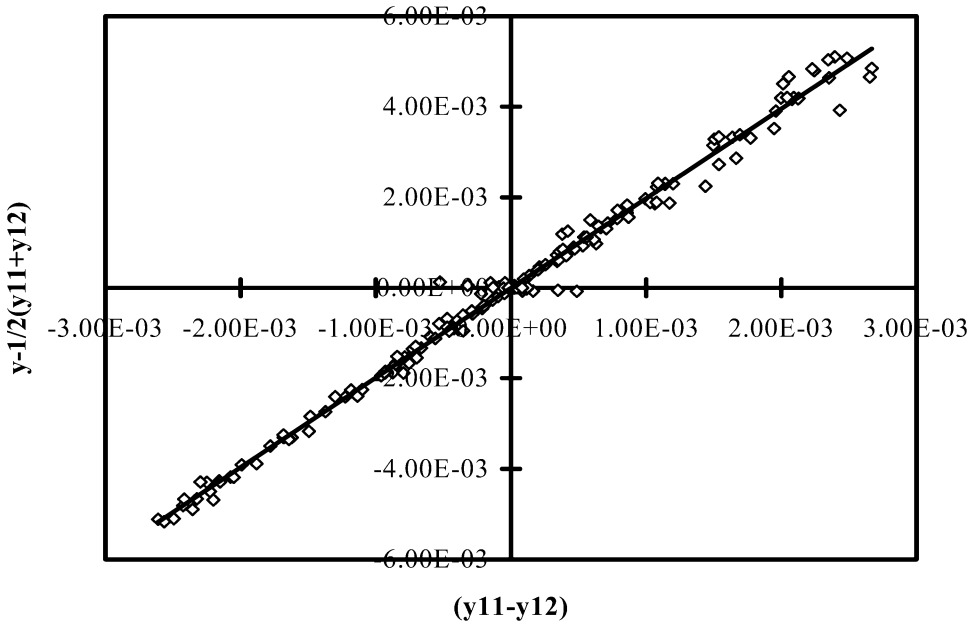

Figure 10. Application of method of nonintrinsic parameter for model discrimination.

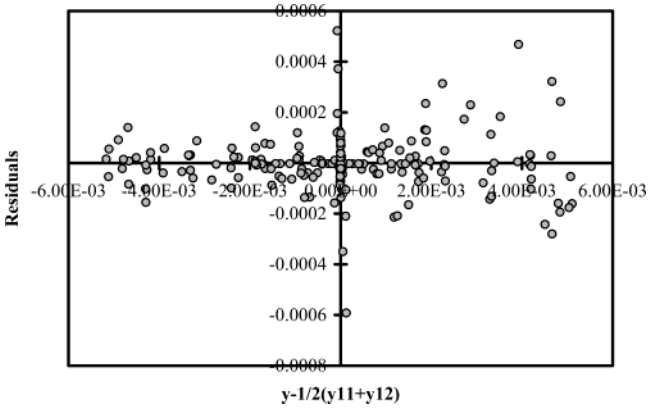

Figure 11. Residuals for the application of method of nonintrinsic parameters for model discrimination.

Table 2. Percent Variation Explained for the Different Proposed Models Considering Pressure Does Not Affect Equilibrium Constant

model	% variation explained
8	98.9
9	99.5
11	99.6
12	99.1

Parameter estimation was performed using *Simusolv*. It was considered that the equilibrium constants were not affected by pressure at constant temperature, and only the kinetic constant for the rate-determining step is influenced by pressure. Our fits showed that the pressure variation of the equilibrium constants were less then one standard deviation and also there is no change in the number of moles with the reaction. Hence it is assumed that the equlibrium constants are pressure independent. Models 1−4 and 9−10 were rejected because of lack of fit of the experimental data. Also, models 5 and 6 were eliminated because the standard deviations of some computed constants were greater than their numerical value.

The remaining models had the %variation explained (basically regression coefficient) presented in Table 2. *Simusolv* calculated the %variation explained according to

$$r^2_{\text{overall}} = \left(1 - \frac{\sum_{j=1}^{m} \text{SSQ}_j}{\sum_{j=1}^{m} \text{SSQ}_{\text{mean}j}}\right)$$

and

$$\text{SSQ}_{\text{mean}j} = \sum_{i=1}^{n} \frac{(y_{i,j} - \bar{y}_j)^2}{f_{i,j}^{\gamma_j}}$$

$$\text{SSQ}_j = \sum_{i=1}^{n} \frac{(y_{i,j} - f_{i,j})^2}{f_{i,j}^{\gamma_j}}$$

with

$$\bar{y}_j = \frac{\sum_{i=1}^{n} \frac{y_{i,j}}{f_{i,j}^{\gamma_j/2}}}{\sum_{i=1}^{n} f_{i,j}^{1/(\gamma_j/2)}}$$

where n is the number of observations, m is the number of variables, y is the experimental value, f is the predicted value, and γ is a weighing parameter.

From Table 2, no discrimination could be done; therefore, statistical methods were employed to discriminate among rival models.

First, the likelihood ratio as a discrimination criterion[25] was used. The ratio of the maximum values of the likelihood function of both models was computed according to the following:

$$\frac{(L_1)_{\max}}{(L_2)_{\max}} = \left(\frac{n - p_i}{n - p_j}\right)^{n/2} \exp\left(\frac{p_i - p_j}{2}\right)\left(\frac{\mathbf{e}_2^{\mathrm{T}}\mathbf{e}_2}{\mathbf{e}_1^{\mathrm{T}}\mathbf{e}_1}\right)^{n/2}$$

Table 3. Residual Sum of Squares for the Proposed Models

model	$\mathbf{e}_i^T\mathbf{e}_i$
8	3.81×10^{-6}
9	3.05×10^{-6}
11	2.66×10^{-6}
12	2.80×10^{-6}

where **e** is the vector of residuals $y - \hat{y}$, n the number of experimental data, and p_i is number of parameters in model i.

For achieving discrimination between models, two number A and B are defined in a way that $0 < B < 1 < A$. These numbers are calculated according to the risk of not rejecting a wrong hypothesis (hyp) according to the following heuristics:

	hyp 1 correct	hyp 2 correct
accept hyp 1	$1 - \zeta$	α
accept hyp 2	ζ	$1 - \alpha$

where ζ and α are small numbers such as 0.05. A and B are calculated as follows:

$$A = \frac{1-\zeta}{\alpha},\ B = \frac{\zeta}{1-\alpha}$$

Finally, the discrimination is performed following these rules:

$$\frac{(L_1)_{max}}{(L_2)_{max}} < B \quad \text{model 1 is rejected}$$

$$\frac{(L_1)_{max}}{(L_2)_{max}} > A \quad \text{model 1 is preferred}$$

$$A < \frac{(L_1)_{max}}{(L_2)_{max}} < B \quad \text{no decision can be made}$$

The model with the smallest residual sum of squares is taken as a reference, and the others models are compared to this reference.

The residual sum of squares for the each model is given in Table 3. Model 11 had the smallest residual sum of squares, so the other models were compared with respect to it.

The following values were obtained:

$$\frac{(L_{11})_{max}}{(L_8)_{max}} = 2.3 \times 10^7$$

$$\frac{(L_{11})_{max}}{(L_9)_{max}} = 314$$

$$\frac{(L_{11})_{max}}{(L_{12})_{max}} = 1.8$$

$$A = 19$$

$$B = 0.0526$$

From these results, models 7 and 8 were discarded. However, no distinction can be made between model 11 and 12.

Then, the method of nonintrinsic parameters[25] was applied. This method supposes that a selection between two nonlinear models must be made:

$$E(y) = f_{11}(x, \beta_{11})$$

$$E(y) = f_{12}(x, \beta_{12})$$

A new dependent variable is defined:

Table 4. Parameter Values of the Kinetic Model for the Hydrogenation of 1-Octene at 50 °C and Substrate to Catalyst Molar Ratio of 400

param	172 bar	207 bar	241 bar
k_3 [=] h^{-1}	$(5.30 \times 10^4) \pm (4.52 \times 10^3)$	$(9.06 \times 10^4) \pm (4.62 \times 10^3)$	$(9.77 \times 10^4) \pm (3.78 \times 10^3)$
k_6 [=] L mol^{-1} h^{-1}	1432 ± 111.3	4541 ± 200.2	4799 ± 129.7
k_{10} [=] L mol^{-1} h^{-1}	826 ± 66.4	2998 ± 133.2	3346 ± 82.6
k_{14} [=] L mol^{-1} h^{-1}	119 ± 17.4	393 ± 21.2	360 ± 11.8
$k_{14'}$ [=] h^{-1}	0	0	0
K_1 [=] L mol^{-1}	3.13 ± 0.199	3.13 ± 0.199	3.13 ± 0.199
K_2 [=] L mol^{-1}	0.15 ± 0.009	0.15 ± 0.009	0.15 ± 0.009
K_5 [=] $L^{1/2}$ $mol^{-1/2}$	8.39 ± 0.176	8.39 ± 0.176	8.39 ± 0.176

Table 5. Parameter Values of the Kinetic Model for the Hydrogenation of 1-Octene at 70 °C and Substrate to Catalyst Molar Ratio of 800

param	172 bar	207 bar	241 bar
k_3 [=] h^{-1}	$(1.29 \times 10^4) \pm (0.26 \times 10^3)$	$(1.47 \times 10^4) \pm (0.86 \times 10^3)$	$(2.83 \times 10^5) \pm (1.09 \times 10^4)$
k_6 [=] L mol^{-1} h^{-1}	4240 ± 151.4	4607 ± 281.8	$(5.66 \times 10^4) \pm (1.33 \times 10^3)$
k_{10} [=] L mol^{-1} h^{-1}	2415 ± 149.6	3079 ± 185.1	$(3.76 \times 10^4) \pm (0.86 \times 10^3)$
k_{14} [=] L mol^{-1} h^{-1}	0 ± 0	29 ± 10.9	1089 ± 27.5
$k_{14'}$ [=] h^{-1}	0	0	0
K_1 [=] L mol^{-1}	4.90 ± 0.153	4.90 ± 0.153	4.90 ± 0.153
K_2 [=] L mol^{-1}	0.32 ± 0.009	0.32 ± 0.009	0.32 ± 0.009
K_5 [=] $L^{1/2}$ $mol^{-1/2}$	7.96 ± 0.079	7.96 ± 0.079	7.96 ± 0.079

Table 6. Parameter Values of the Kinetic Model for the Hydrogenation of 1-Octene at 95 °C and Substrate to Catalyst Molar Ratio of 800

param	172 bar	207 bar	241 bar
k_3 [=] h^{-1}	$(1.70 \times 10^5) \pm (0.65 \times 10^4)$	$(2.00 \times 10^5) \pm (0.49 \times 10^4)$	$(4.09 \times 10^5) \pm (0.83 \times 10^4)$
k_6 [=] L mol^{-1} h^{-1}	$(4.31 \times 10^4) \pm (1.32 \times 10^3)$	$(5.84 \times 10^4) \pm (1.55 \times 10^3)$	$(1.27 \times 10^5) \pm (0.32 \times 10^4)$
k_{10} [=] L mol^{-1} h^{-1}	$(2.84 \times 10^4) \pm (1.11 \times 10^3)$	$(3.28 \times 10^4) \pm (1.07 \times 10^3)$	$(7.14 \times 10^4) \pm (1.75 \times 10^3)$
k_{14} [=] L mol^{-1} h^{-1}	$(1.21 \times 10^3) \pm (0.089 \times 10^3)$	$(2.05 \times 10^3) \pm (0.061 \times 10^3)$	$(4.10 \times 10^3) \pm (0.145 \times 10^3)$
$k_{14'}$ [=] h^{-1}	0	0	0
K_1 [=] L mol^{-1}	4.69 ± 0.189	4.69 ± 0.189	4.69 ± 0.189
K_2 [=] L mol^{-1}	0.44 ± 0.014	0.44 ± 0.014	0.44 ± 0.014
K_5 [=] $L^{1/2}$ $mol^{-1/2}$	8.38 ± 0.208	8.38 ± 0.208	8.38 ± 0.208

Table 7. Arrhenius Parameter Estimation for the Rate-Determining Step Constants at Given Pressures

	172 bar		207 bar		241 bar	
param	A	E_a/R [K]	A	E_a/R [K]	A	E_a/R [K]
k_3	1.09×10^{10}	4255	7.31×10^8	3226	3.53×10^{10}	4135
k_6	7.10×10^{16}	1.04×10^4	1.61×10^4	8098	2.45×10^{16}	9450
k_{10}	1.48×10^{17}	1.08×10^4	2.29×10^{13}	7585	2.20×10^{15}	8772
k_{14}	8.31×10^5	2903	9.89×10^4	2167	1.99×10^7	3503

Table 8. Parameter Values of the Kinetic Model for the Hydrogenation of Cyclohexene Using the Catalyst $RhCl(TAN_{15}DPPA)_3$ with 30% of Oxidized Phosphines at 172 bar

param	343 K	368 K	393 K
k_3 [=] h^{-1}	319 ± 16.9	$(1.66 \times 10^4) \pm (2.22 \times 10^3)$	$(9.06 \times 10^4) \pm (1.236 \times 10^4)$
k_{14} [=] L mol^{-1} h^{-1}	3.4 ± 1.41	149 ± 27.3	370 ± 58.6
$k_{14'}$ [=] h^{-1}	0	0	0
K_1 [=] L mol^{-1}	2.16 ± 0.107	2.09 ± 0.121	0.70 ± 0.026
K_2 [=] L mol^{-1}	1.94 ± 0.072	2.00 ± 0.105	3.49 ± 0.125
K_5 [=] $L^{1/2}$ $mol^{-1/2}$	7.96 ± 0.079	8.38 ± 0.208	8.38 ± 0.208

$$z = y - \frac{1}{2}(\hat{y}_{11} + \hat{y}_{12})$$

where $\hat{y}_i$ is the prediction of the dependent variable y under model i.

After some mathematical steps, the following is obtained:

$$E(z) = \lambda(\hat{y}_{11} - \hat{y}_{12})$$

If model 11 is correct, λ takes a value of +0.5, but if model 12 is correct, its value is −0.5. Regression of z on $(\hat{y}_1 - \hat{y}_2)$ determines which model is best.

Figure 10 presents the plot between $(\hat{y}_1 - \hat{y}_2)$ vs z. Doing linear regression, a value of 0.500 (±0.0065) was calculated for the slope; moreover, Figure 11 shows that the residuals are evenly distributed along the dependent variable confirming the excellent regression analysis. Therefore, model 11 was preferred over model 12.

Thus, if the rate-determining steps are reaction 3 for hydrogenation, and 6 and 10 for isomerization, the following kinetic equations can be derived:

$$\frac{dC_P}{dt} = \frac{k_3 K_1 K_2 C_A C_B C_{cat}}{1 + (1 + K_2 C_A) K_1 C_B + K_5^{1/2} C_B^{1/2}}$$

$$\frac{dC_C}{dt} = \frac{k_6 K_5^{1/2} C_A C_B^{1/2} C_{cat}}{1 + (1 + K_2 C_A) K_1 C_B + K_5^{1/2} C_B^{1/2}}$$

$$\frac{dC_D}{dt} = \frac{k_{10} K_5^{1/2} C_A C_B^{1/2} C_{cat}}{1 + (1 + K_2 C_A) K_1 C_B + K_5^{1/2} C_B^{1/2}}$$

$$\frac{dC_{cat}}{dt} = \frac{k_{14} C_A C_{cat}}{1 + (1 + K_2 C_A) K_1 C_B + K_5^{1/2} C_B^{1/2}} - k_{14'} C_{dcat}$$

$$C_A = C_{A0} - C_P - C_C - C_D$$

$$C_B = C_{B0} - C_P$$

$$C_{dcat} = C_{cat0} - C_{cat}$$

where

A = 1-octene

B = hydrogen

P = *n*-octane

C = (*E*)2-octene

D = (*Z*)2-octene

The values of the parameters are reported in Tables 4−6 for all the studied experimental conditions.

Figures 12−14 show the comparison of calculated and experimental results for the hydrogenation of 1-octene at all the studied experimental conditions. As can be concluded from these figures, the kinetic model was found to be consistent with the general profiles of all the products.

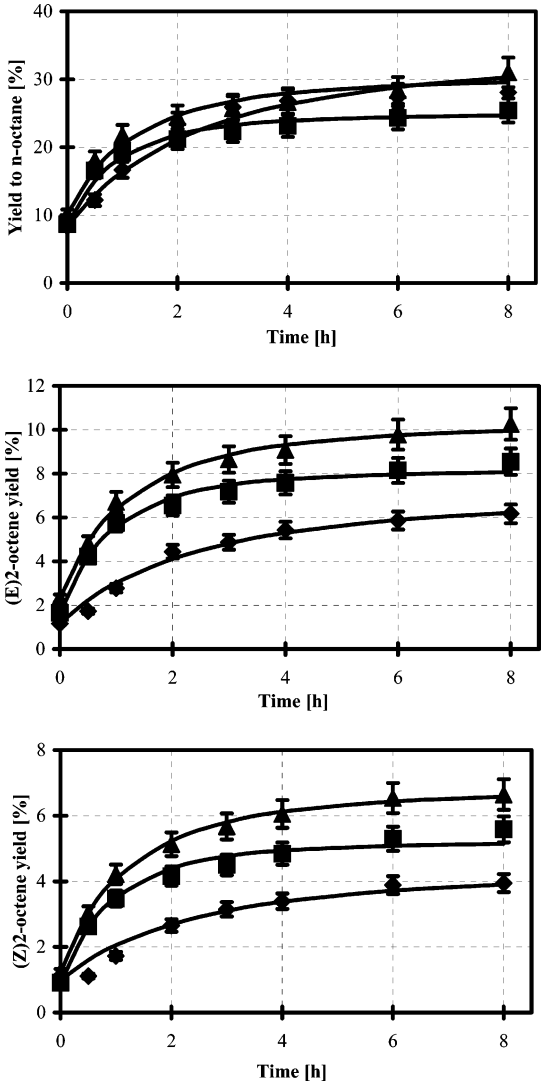

Figure 12. Comparison between the experimental and calculated results for the hydrogenation of 1-octene at 50 °C: (◆) 172 bar, (■) 207 bar, (▲) 241 bar, (—) calcd.

Table 9. Arrhenius Parameter Estimation for the Rate-Determining Step Constant of the Hydrogenation of Cyclohexene at 172 bar

constant	A	E_a/R [K]
k_3	1.13×10^{22}	1.53×10^4
k_{14}	8.13×10^{16}	1.28×10^4

The dependence on temperature for the rate-determining step constants was determined at each pressure by applying the Arrhenius equation in the following way:

$$\ln k = -\frac{E_a}{R}\left(\frac{1}{T} - \frac{1}{T_0}\right) + \ln k^0$$

where T_0 is the mid-temperature for the temperature range considered, $k^0 = A \times \exp(-E_a/RT_0)$, E_a is the activation energy, and A is the frequency factor.

The obtained results for the frequency factor and activation energy for each constant are reported in Table 7. The confidence interval limits of the frequency factor and activation energy are not reported because in many cases this confidence interval was greater than the value itself. This was obtained due to the poor fitting of the rate constants with respect to Arrhenius equation.

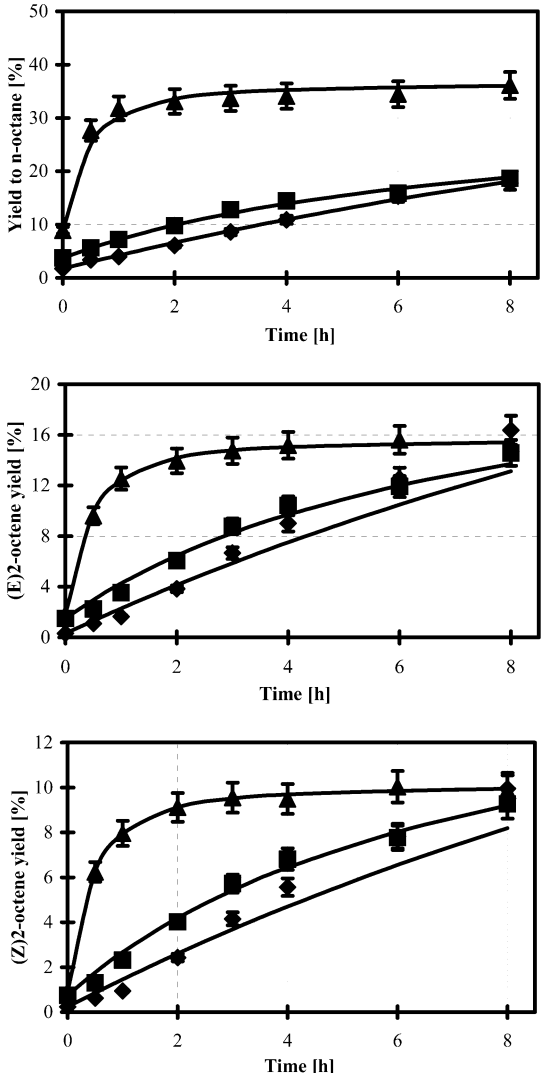

Figure 13. Comparison between the experimental and calculated results for the hydrogenation of 1-octene at 70 °C: (◆) 172 bar, (■) 207 bar, (▲) 241 bar, (—) calcd.

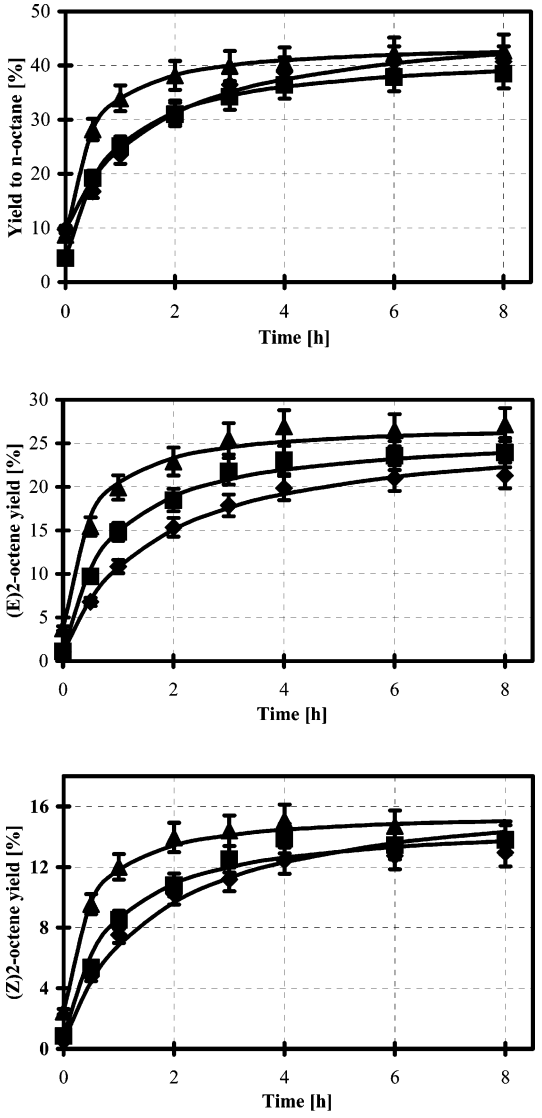

Figure 14. Comparison between the experimental and calculated results for the hydrogenation of 1-octene at 95 °C: (◆) 172 bar, (■) 207 bar, (▲) 241 bar, (—) calcd.

However, this lack of fitness is attributed to the experimental error obtained during the collection of data, and also to the shortage of experiments at different temperatures. Only three temperatures were analyzed, which are not sufficient to have conclusive results; therefore, more experiments at different temperatures within the studied interval should be performed.

The same kinetic mechanism was employed to determine the kinetic parameters for the hydrogenation of cyclohexene using the catalyst $RhCl(TAN_{15}DPPA)_3$ with 30% of oxidized phosphines. The temperature range studied was 70−120 °C at 172 bar. The substrate to catalyst molar ratio was 400 at 70 °C, and 700 at 95 and 120 °C. The initial mole fraction of reactants was kept constant in all the experiments at different temperatures.

In this case, the formation of monohydride catalytic species is taken into consideration even though no isomerization products were detected. This was done in order to keep the same kinetic mechanism. The double bond in cyclohexene may be shifting around, but it does not produce a distinct new isomer.

If reaction 3 is considered the rate controlling for hydrogenation, then the following kinetic equations are obtained:

$$\frac{dC_P}{dt} = \frac{k_3 K_1 K_2 C_A C_B C_{cat}}{1 + (1 + K_2 C_A) K_1 C_B + K_5^{1/2} C_B^{1/2}}$$

$$\frac{dC_{cat}}{dt} = \frac{k_{14} C_A C_{cat}}{1 + (1 + K_2 C_A) K_1 C_B + K_5^{1/2} C_B^{1/2}} - k_{14'} C_{dcat}$$

$$C_A = C_{A0} - C_P$$

$$C_B = C_{B0} - C_P$$

$$C_{dcat} = C_{cat0} - C_{cat}$$

where

A = cyclohexene

B = hydrogen

P = cyclohexane

Table 8 presents the values of the estimated parameters, and Figure 15 shows the comparison between the

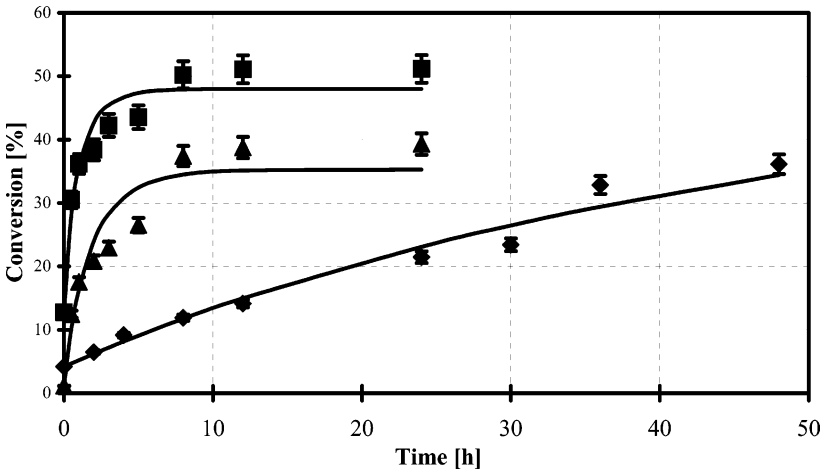

Figure 15. Comparison between the experimental and calculated results for the hydrogenation of cyclohexene using the catalyst RhCl-$(TAN_{15}DPPA)_3$ with 30% of oxidized phosphines at 172 bar: (◆) 343 K, (▲) 368 K, (■) 393 K, (—) calcd.

calculated and the experimental results. Once more, the calculated values fit very well the experimental data.

Again, the dependence on temperature of the rate-determining step constant was determined using the Arrhenius equation. The results are presented in Table 9.

One more time, lack of fitness of rate-determining step constant with respect to the Arrhenius equation was obtained for the same reasons explained above.

Conclusions

A mechanism cycle was proposed for the hydrogenation and isomerization of 1-octene, and for the hydrogenation of cyclohexene. Statistical methods were applied to discriminate among rival models. It was proposed that two hydride catalytic species are formed during the reaction cycle: dihydride species for promoting hydrogenation, and monohydride species for yielding isomerization. Also, deactivation of the catalyst was attributed to the formation of unsaturated olefin complex on the catalyst. It was found that the rate-determining step for hydrogenation was the migratory insertion of hydrogen into the olefin to produce an alkylrhodium hydride complex. Moreover, the rate-determining step for isomerization was considered to be the coordination of the olefin in the monohydride catalytic species. The final kinetic model was found to be consistent with the general trends of the experimental data for both the hydrogenation and isomerization of 1-octene and cyclohexene.

Acknowledgment

This work was supported by The Environmental Protection Agency (EPA), Gulf Coast Hazardous Substance Research Center, Consejo Nacional de Ciencia y Tecnologia (CONACYT) of Mexico, and The Scientific and Technical Research Council of Turkey (TUBITAK-NATO). The authors are grateful for partial support from each organization.

Literature Cited

(1) Lancaster, M. In *Handbook of Green Chemistry & Technology*; Clark, J., Macquarrie, D., Eds.; Blackwell Science Ltd.: Malden, MA, 2002; pp 10−27.

(2) Cornils, B.; Hermann, W. A. In *Applied Homogeneous Catalysis with Organometallic Compounds*; Cornils, B., Hermann, W. A., Eds.; Wiley-VCH: Verlag GmbH, Weinheim, Germany, 1996; pp 1−25.

(3) Leitner, W. In *Modern Solvents in Organic Synthesis*; Knochel, P., Ed.; Topics in Current Chemistry; Springler-Verlag: Berlin, Germany, 1999; Vol. 206, pp 107−132.

(4) Jessop, P. G.; Ikariya, T.; Noyori, R. Homogeneous Catalysis in Supercritical Fluids. *Chem. Rev.* **1999**, *99*, 475−493.

(5) Baiker, A. Supercritical Fluids in Heterogeneous Catalysis. *Chem. Rev.* **1999**, *99*, 453−473.

(6) Oakes, R. S.; Clifford, A. A.; Rayner, C. M. The Use of Supercritical Fluids in Synthetic Organic Chemistry. *J. Chem. Soc., Perkin Trans. 1* **2001**, *9*, 917−941.

(7) Subramaniam, B.; Lyon, C. J.; Arunajatesan, V. Environmentally Benign Multiphase Catalysis with Dense Phase Carbon Dioxide. *Appl. Catal., B* **2002**, *37*, 279−292.

(8) Savage, P. E.; Gopalan, S.; Mizan, T. I.; Martino, C. J.; Brock, E. E. Reactions at Supercritical Conditions: Applications and Fundamentals. *AIChE J.* **1995**, *41*, 1723−1778.

(9) Sarbu, T.; Styranec, T. J.; Beckman, E. J. Design and Synthesis of Low Cost, Sustainable CO_2-philes. *Ind. Eng. Chem. Res.* **2000**, *39*, 4678−4683.

(10) Bergbreiter, D. E.; Franchina J. G.; Case, B. L. Fluoroacrylate-Bound Fluorous-Phase Soluble Hydrogenation Catalysts. *Org. Lett.* **2000**, *2*, 393−395.

(11) Chen, W.; Xu, L.; Xiao, J. Palladium-Catalyzed Synthesis of Aqueous, Fluorous, and Supercritical CO_2-Soluble Phosphines. *Org. Lett.* **2000**, *2*, 2675−2677.

(12) Fawcett, J.; Hope, E. G.; Kemmit, R. D.; Paige, D. R.; Russell, D. R.; Stuart, A. M.; Cole-Hamilton, D. J.; Payne, M. J. Fluorous-phase soluble rhodium complexes: X-ray structure of $[RhCl(CO)(P(C_2H_4C_6F_{13})_3)_2]$. *Chem. Commun.* **1997**, *12*, 1127−1128.

(13) Kainz, S.; Koch, D.; Baumann, W.; Leitner, W. Perfluoroalkyl-Substituted Arylphosphanes as Ligands for Homogeneous Catalysis in Supercritical Carbon Dioxide. *Angew. Chem., Int. Ed. Engl.* **1997**, *36*, 1628−1630.

(14) Richter, B.; Deelman, B. J.; Van Koten, G. Fluorous biphasic hydrogenation of 1-alkenes using novel derivatives of Wilkinson's catalyst. *J. Mol. Catal. A: Chem.* **1999**, *145*, 317−321.

(15) Kani, I.; Omary, M. A.; Rawashdeh-Omary, M. A.; Lopez-Castillo, Z. K.; Flores, R.; Akgerman, A.; Fackler, J. P., Jr. Homogeneous catalysis in supercritical carbon dioxide with rhodium catalysts tethering fluoroacrylate polymer ligands. *Tetrahedron* **2002**, *58*, 3923−3928.

(16) Lopez-Castillo, Z. K.; Flores, R.; Kani, I.; Fackler, J. P., Jr.; Akgerman, A. Fluoroacrylate Copolymer Supported Rhodium

Catalysts for Hydrogenation Reactions in Supercritical Carbon Dioxide. *Ind. Eng. Chem. Res.* **2002**, *41*, 3075−3080.

(17) Li, L. X.; Kiran, E. Estimation of critical properties of binary-mixtures using group contribution methods. *Chem. Eng. Commun.* **1990**, *94*, 131−141.

(18) Liu, Z. Y. Prediction of critical pressure of dilute multicomponent mixtures. *AIChE J.* **1998**, *44*, 1709−1712.

(19) Halpern, J. Mechanistic Aspects of Homogeneous Catalytic Hydrogenation and Related Processes. *Inorg. Chim. Acta* **1981**, *50*, 11−19.

(20) Collman, J. P. *Principles and applications of organotransition metal chemistry*; University Science Books: Mill Valley, CA, 1980.

(21) Sanchez-Delgado, R. A.; Rosales, M. Kinetics studies as a tool for the elucidation of the mechanisms of methal complex-catalyzed homogeneous hydrogenation reactions. *Coord. Chem. Rev.* **2000**, *196*, 249−280.

(22) Khan, M. M.; Khan, B. T.; Begum, S. Thermodynamics of the Hydrogenation of Olefins Catalyzed by Rh(I) and Ir(I) Complexes. *J. Mol. Catal.* **1986**, *34*, 9−18.

(23) Schrock, R. R.; Osborn, J. A. Catalytic-Hydrogenation using Cationic Rhodium Complexes.1. Evolution of Catalytic System and Hydrogenation of Olefins. *J. Am. Chem. Soc.* **1976**, *98*, 2134−2143.

(24) Buriak, J. M.; Klein, J. C.; Herrington, D. G.; Osborn, J. A. Probing the mechanisms of enantioselective hydrogenation of simple olefins with chiral rhodium catalysts in the presence of anions. *Chem.—Eur. J.* **2000**, *6*, 139−150.

(25) Froment, G. M.; Hosten, L. In *CATALYSIS—Science and Technology*; Anderson, J. R., Boudart, M., Eds.; Springler-Verlag: Berlin, Germany, 1981; Vol. 2, pp 97−170.

Received for review April 14, 2003
Revised manuscript received September 30, 2003
Accepted October 9, 2003

IE0303202